Numerical study of scattering from rough inhomogeneous films

H. Giovannini

Laboratoire d'Optique des Surfaces et des Couches Minces, Unité Propre de Recherche de l'Enseignement Supérieur Associée 6080, Centre National de la Recherche Scientifique, Ecole Nationale Supérieure de Physique de Marseille, 13397 Marseille Cedex 20, France

M. Saillard

Laboratoire d'Optique Electromagnétique, Unité Propre de Recherche de l'Enseignement Supérieur Associée 6079, Centre National de la Recherche Scientifique, Faculté des Sciences et Techniques de Saint Jérôme, Service 262 13397 Marseille Cedex 20, France

A. Sentenac

Laboratoire d'Optique des Surfaces et des Couches Minces, Unité Propre de Recherche de l'Enseignement Supérieur Associée 6080, Centre National de la Recherche Scientifique, Ecole Nationale Supérieure de Physique de Marseille, 13397 Marseille Cedex 20, France

Received July 24, 1997; revised manuscript received November 24, 1997; accepted December 17, 1997

We adapt the differential method to the study of scattering from randomly rough inhomogeneous films, and we extend the application domain of the surface-integral method to rough surfaces with many embedded scatterers. These methods are compared in the case of geometries in which both volume and surface scattering occur. A good agreement is obtained, and the advantages and drawbacks of each technique are pointed out. The angular scattering from rough inhomogeneous structures corresponding to models of snowcover in the radio-frequency domain or paints in the optical domain is shown. © 1998 Optical Society of America [S0740-3232(98)02105-X]

OCIS codes: 240.6700, 290.0290, 290.5880.

1. INTRODUCTION

The study of electromagnetic surface and volume scattering is of current importance in several domains. This issue arises in geophysics, for microwave sensing of snow, ice, ocean surfaces, or soils, but also in optics, where the performance of components has to be improved to reduce the amount of scattered light.[1,2] More generally, to interpret or to optimize the scattering signature of a rough inhomogeneous medium, one must be able to handle accurately the associated forward-diffraction problem.

Volume and surface scattering are both difficult problems that are usually studied separately. Most often, approximate methods, such as the first-order perturbation theory,[3] transfer radiative equation,[4] and Born approximation[5,6] are proposed to combine both effects. These methods are commonly used, but in some cases poor agreement is found between experimental and numerical results.[7,8] It is then necessary to know whether the validity of the scatterer's physical description has to be questioned or whether it is the method of computation and the approximations used that have to be revised. In the latter case, a comparison between the results obtained with the approximate method and those given by a rigorous one is essential.

In this paper we present two methods, based on rigorous theories, that calculate the scattering of electromagnetic waves from two-dimensional structures (invariant along one axis). These methods are well suited to the study of rough inhomogeneous films. The first technique is based on a differential formalism that is widely used in the grating domain.[9] This method, which has been largely improved with the S-matrix (or R-matrix) algorithm,[10,11] permits one to treat the case of rough films with both localized inhomogeneities (brine pockets, air bubbles, etc.) and inhomogeneities that are described by continuous permittivity fluctuations. Thanks to a representation in the Fourier space, surface and volume scattering are handled in the same way. The second technique is based on a rigorous boundary-integral formalism. We extended the application domain of the method presented in Ref. 12 to the issue of scattering from rough surfaces with a high number of embedded scatterers. Here the field scattered by small cylindrical objects is accurately described with a few terms in Rayleigh expansions. A mixed representation in both coordinate and spectral domains allows us to treat rigorously the problem of scattering from rough structures with many buried objects, at a lower computational cost than with a volume finite-element method.[13]

Our aim in this paper is to present and compare these methods by showing their respective advantages. Comparisons of the numerical results are drawn. It is shown

that it is possible to determine the influence, on the differential reflection coefficient (DRC), of the optogeometrical parameters of rough inhomogeneous films. Examples are given for various cases in both the optical domain and the radio-frequency domain.

2. GEOMETRY OF THE PROBLEM

We study the scattering from electromagnetic waves by structures that are invariant along the y axis (see Fig. 1). We consider both s polarization (the electric field is parallel to the y axis) and p polarization (the magnetic field is parallel to the y axis). Generally, the scattering geometry is described by a randomly (or not) perturbed region of thickness D and length L, embedded in two semi-infinite homogeneous media. The dielectric constant ε_t of the whole system is given by

$$\varepsilon_t(x, z) = \varepsilon_1 \quad \text{if } z > D, \tag{1a}$$

$$\varepsilon_t(x, z) = \varepsilon(x, z) \quad \text{if } 0 < z < D, \tag{1b}$$

$$\varepsilon_t(x, z) = \varepsilon_2 \quad \text{if } z < 0. \tag{1c}$$

The perturbed region may be a rough surface, an inhomogeneous film, or an object buried under a rough surface, depending on the function $\varepsilon(x, z)$.

The system is illuminated with a monochromatic Gaussian beam of angular frequency ω. Throughout this paper the time dependence $\exp(-i\omega t)$ is omitted from the equations. In the semi-infinite homogeneous media the y component of the electric field in s polarization, or the y component of the magnetic field, in p polarization, denoted by F, satisfies the wave equation

$$\nabla^2 F + k_j^2 F = 0, \tag{2}$$

where $k_j^2 = \varepsilon_j \omega^2/c^2$, with $j = 1$ for $z > D$ and $j = 2$ for $z < 0$.

The incident field is given by

$$F_{\text{inc}}(x, z) = \int P(\alpha - \alpha_{\text{inc}}) \exp[i\alpha x - i\gamma_1(\alpha)(z - z_0)]\,\mathrm{d}\alpha, \tag{3}$$

where

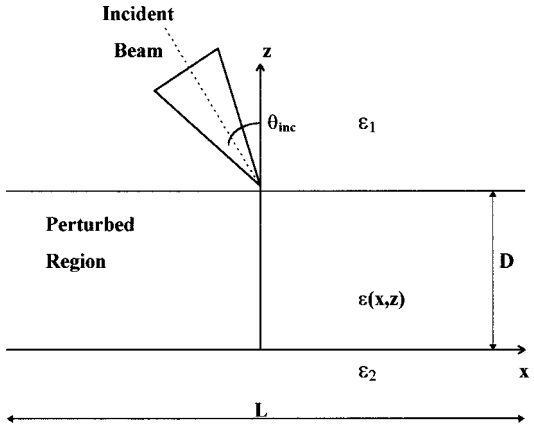

Fig. 1. Geometry of the problem. Throughout the paper the geometries are invariant along the y axis, and they are illuminated under normal incidence by a Gaussian beam of waist $w = 1$ [Eq. (4a)].

$$P(\alpha) = w \exp(-w^2\alpha^2/2), \tag{4a}$$

$$\gamma_j(\alpha) = (k_j^2 - \alpha^2)^{1/2}, \qquad \mathrm{Im}(\gamma_j) > 0,\ j = 1, 2, \tag{4b}$$

where $\mathrm{Im}(x)$ signifies the imaginary part of a complex number x and

$$\alpha_{\text{inc}} = k_1 \sin \theta_{\text{inc}}. \tag{4c}$$

The parameters w (beam waist), α_{inc}, and z_0 are used to modify the angular width, the mean angle of incidence θ_{inc}, and the position of the beam waist of the incident field.

For $z > D$, the field can be cast in the form

$$F(x, z) = F_{\text{inc}}(x, z) + \int f_1(\alpha) \exp[i\alpha x + i\gamma_1(\alpha) z]\,\mathrm{d}\alpha. \tag{5a}$$

For $z < 0$ we have

$$F(x, z) = \int f_2(\alpha) \exp[i\alpha x - i\gamma_2(\alpha) z]\,\mathrm{d}\alpha, \tag{5b}$$

where f_1 and f_2 are the amplitudes to be calculated from the plane-wave expansion. The DRC and the differential transmission coefficient (DTC), which give the fraction of the total incident energy that is scattered into an angular interval $\delta\theta_s$ about the scattering direction defined by the scattering angle θ_s, are given by[13]

$$\frac{\partial R}{\partial \theta_s} = \frac{|\gamma_1(\alpha_s) f_1(\alpha_s)|^2}{P_{\text{inc}}}, \tag{6a}$$

$$\frac{\partial T}{\partial \theta_s} = \frac{|\gamma_2(\alpha_s) f_2(\alpha_s)|^2}{P_{\text{inc}}}, \tag{6b}$$

where $\alpha_s = k_1 \sin \theta_s$ for the reflection and $\alpha_s = k_2 \sin \theta_s$ for the transmission. P_{inc} is the total incident flux through the plane $z = D$ (see Fig. 1),

$$P_{\text{inc}} = \int |P(\alpha - \alpha_{\text{inc}}) \gamma_1(\alpha)|^2 \mathrm{d}\alpha. \tag{7}$$

In Section 5 we study deterministic and stochastic geometries. In the latter case we introduce the mean DRC $\langle \partial R/\partial \theta_s \rangle$, which is calculated through ensemble averaging (Monte Carlo simulations).

3. DIFFERENTIAL METHOD

This formalism has been widely used in the grating domain, but it has also been extended to a nonperiodic obstacle[14] for s polarization. Its main advantage is that the geometry of the system is described in a very general way, with the variations of the permittivity $\varepsilon(x, z)$. The fact that those fluctuations may stem from the presence of rough surfaces, buried objects, or bubbles has no impact on the numerical scheme. Unfortunately, until recently, this versatile technique was plagued by numerical instabilities that restricted its domain of application and its significance. The introduction of the R- or S-matrix algorithm[10,11] in 1994, which has permitted researchers to overcome those difficulties, has been decisive in the revival of interest for this method. In the following we briefly recall its main steps.

A. *S* Polarization

In the perturbed region, $0 < z < D$, the y component $E(x, z)$ of the electric field satisfies the wave equation

$$\nabla^2 E + k^2(x, y)E = 0, \tag{8}$$

where $k^2(x, z) = \varepsilon(x, z)\omega^2/c^2$. To define $k^2(x, z)$ more precisely, we assume that it can be written as

$$k^2(x, z) = k^2(z) + \Delta k^2(x, z), \tag{9}$$

with $\Delta k^2(x, z) = 0$ if $|x| > L/2$. Hence the x variations of the permittivity are restricted to an interval of length L. When dealing with allegedly infinite rough surfaces, we take to be L much larger than the illuminated section by the Gaussian beam, to minimize edge effects. Let $e(\alpha, z)$ and $\Delta\kappa^2(\alpha, z)$ be the Fourier transforms at constant z of $E(x, z)$ and $\Delta k^2(x, z)$, respectively,

$$E(x, z) = \int e(\alpha, z)\exp(i\alpha x)\mathrm{d}\alpha, \tag{10}$$

$$\Delta k^2(x, z) = \int \Delta\kappa^2(\alpha, z)\exp(i\alpha x)\mathrm{d}\alpha. \tag{11}$$

Inserting Eqs. (10) and (11) into Eq. (8) leads us to an integro-differential equation of the second order for $e(\alpha, z)$,

$$\frac{\partial^2 e(\alpha, z)}{\partial z^2} + [k^2(z) - \alpha^2]e(\alpha, z) + \int \Delta\kappa(\alpha - \alpha', z)e(\alpha', z)\mathrm{d}\alpha' = 0. \tag{12}$$

We can transform this equation into a differential system of the first order by introducing the variable $[\partial e(\alpha, z)]/\partial z$. Knowledge of the field and its derivative at a given ordinate $z \in [0, D]$, $\{e(\alpha, z), [\partial e(\alpha, z)]/\partial z\}$ (for all α) allows us, by integrating Eq. (12), to calculate, at any ordinate $z' \in [0, D]$, $\{e(\alpha, z'), [\partial e(\alpha, z')]/\partial z\}$ (for all α). The continuity of E and $\partial E/\partial z$ at $z = 0$ and $z = D$ is then used to evaluate the scattered amplitudes $f_1(\alpha)$ and $f_2(\alpha)$ as defined in [Eq. (5)]. However, to calculate the linear relationship between $\{e(\alpha, z), [\partial e(\alpha, z)]/\partial z\}$, and $\{e(\alpha, z'), [e(\alpha, z'),]\partial z\}$, one has to transform Eq. (12) into a finite set of differential equations by discretizing and truncating the Fourier representations of the field E and of Δk^2. Finally, the relationship between the field at z and the field at z' can be written, in matrix notation, as

$$\begin{bmatrix} \mathbf{e} \\ \dfrac{\partial \mathbf{e}}{\partial \alpha} \end{bmatrix}(z) = \underline{\mathbf{T}}(z, z')\begin{bmatrix} \mathbf{e} \\ \dfrac{\partial \mathbf{e}}{\partial \alpha} \end{bmatrix}(z'), \tag{13}$$

where

$$\mathbf{e}(z) = \begin{bmatrix} e(-N\Delta\alpha, z) \\ \vdots \\ e(N\Delta\alpha, z) \end{bmatrix}.$$

In Eq. (13), $\Delta\alpha$ is the step of discretization, and $\alpha_{\max} = N\Delta\alpha$ is the highest spatial frequency that is retained in the description of the field. The matrix $\underline{\mathbf{T}}$ is obtained by computation with a Runge–Kutta algorithm, of the images of $2N-1$ independent vectors.[9] Note that, for large values of D, the transmission matrix $\underline{\mathbf{T}}(0, D)$ is not well calculated because of the decaying and increasing exponentials that are involved in the integration. It is thus necessary to decompose the perturbed region in N_p elementary slices with sufficiently small thickness d, $(D = N_p d)$. When one correctly evaluates $\underline{\mathbf{T}}[(p-1)d, pd]$, $p \in [1, N_p]$, one can deduce the corresponding scattering matrix $\underline{\mathbf{S}}_p$.[10,11] The global scattering matrix $\underline{\mathbf{S}} = \Pi_{p=1}^{N_p}\underline{\mathbf{S}}_p$ relates the impinging waves on the scatterer (i.e., the perturbed region) to the outgoing ones. Hence we get a linear system that links the reflected and transmitted outgoing plane waves to the incident ones,

$$\begin{bmatrix} f_1(-N\Delta\alpha) \\ \vdots \\ f_1(N\Delta\alpha) \\ f_2(-N\Delta\alpha) \\ \vdots \\ f_2(N\Delta\alpha) \end{bmatrix} = \underline{\mathbf{S}}\begin{bmatrix} 0 \\ \vdots \\ 0 \\ P(-N\Delta\alpha - \alpha_{\mathrm{inc}}) \\ \vdots \\ P(N\Delta\alpha - \alpha_{\mathrm{inc}}) \end{bmatrix}. \tag{14}$$

Note that the Fourier transform of the incident field [Eq. (3)] has been discretized and truncated in the same way as that of the field inside the perturbed region [Eq. (10)]. Once f_1 and f_2 are known, we can evaluate the differential reflection and the transmission coefficients by using Eq. (6).

B. *P* Polarization

A similar treatment is used for p polarization. The main difference lies in the differential equation satisfied by the y component of the magnetic field H,

$$\frac{\partial}{\partial x}\left(\frac{1}{k^2}\frac{\partial H}{\partial x}\right) + \frac{\partial}{\partial z}\left(\frac{1}{k^2}\frac{\partial H}{\partial z}\right) + H = 0. \tag{15}$$

This equation is rewritten as a differential system of the first order so that the continuously derivable product $\tilde{E} = [(1/k^2)\ (\partial H/\partial z)]$ is never split,

$$\frac{\partial H}{\partial z} = k^2\tilde{E}, \tag{16a}$$

$$\frac{\partial \tilde{E}}{\partial z} = -\frac{\partial}{\partial x}\left(\frac{1}{k^2}\frac{\partial H}{\partial x}\right) - H. \tag{16b}$$

Assuming that the x variations of the permittivity are restricted to a finite interval of length L, we put $1/k^2$ in the form

$$\frac{1}{k^2}(x, z) = \frac{1}{k^2}(z) + \Delta\frac{1}{k^2}(x, z), \tag{17}$$

with

$$\Delta\frac{1}{k^2}(x, z) = 0 \quad \text{if } |x| > L/2.$$

By introducing the Fourier transforms $h(\alpha, z)$, $\tilde{e}(\alpha, z)$ $\Delta\kappa,(\alpha, z)$, $\Delta(1/\kappa^2)(\alpha, z)$ of $H(x, z)$, $\tilde{E}(x, z)$, Δk, $\Delta(1/k^2)$, respectively, we can write the system (16) in the Fourier space as

$$\frac{\partial h}{\partial z}(\alpha, z) = k^2(z)\tilde{e}(\alpha, z) + \int \Delta\kappa(\alpha - \alpha', z)\tilde{e}(\alpha', z)\mathrm{d}\alpha', \tag{18a}$$

$$\frac{\partial \tilde{e}}{\partial z}(\alpha, z) = h(\alpha, z)\left[\alpha^2 \frac{1}{k^2}(z) - 1\right] + \alpha \int \alpha' \Delta \frac{1}{\kappa^2}(\alpha - \alpha', z)h(\alpha', z)\mathrm{d}\alpha'. \tag{18b}$$

This coupled differential system of the first order and the continuity of H and $\tilde{E}$ at $z = 0$ and $z = D$ allows us to calculate the scattering matrix of the perturbed region with the same method as that described for s polarization.

C. Validation of the Results

The numerical implementation of the differential formalism is straightforward, but it requires a careful testing of all the parameters that are introduced in the quantization and truncation of the Fourier transforms, in the Runge–Kutta algorithm, and in the S-matrix algorithm. Note that, if the Fourier transform of the field is truncated at $\alpha_{\max}$, the highest spatial frequency needed for $\Delta\kappa$ and $\Delta(1/\kappa^2)$ is $2\alpha_{\max}$. In general the evaluations of $\Delta\kappa$, $\Delta(1/\kappa^2)$ are performed with a fast-Fourier-transform technique. In this case the parameters L, N, and $\Delta\alpha$ are linked by the relation $2(2N + 1)2\pi = L\Delta\alpha$. For the results presented in Section 5, convergence was usually reached with $\Delta\alpha = k_1/20$ and $\alpha_{\max} = 5k_1$. These values correspond to $N = 128$ and $L = 16\lambda_1$, where λ_1 is the wavelength in the upper medium. However, in some cases, where the scattering structures are very small (scatterers in snow), it was necessary to increase $\alpha_{\max}$ up to $10k_1$. In the Runge–Kutta algorithm an integration step $\Delta z = \lambda_1/10$ was sufficient, and in the S-matrix algorithm a decomposition of the perturbed region into slices of thickness $d = \lambda_1/3$ was enough. Note that these parameters need to be tested systematically against convergence because they clearly depend on the values of the permittivity (we studied dielectrics with permittivities smaller than 9). Energy conservation was satisfied up to 10^{-6} in the lossless cases, but this test is not representative of the accuracy of the results.

The results given by the differential method are compared with those of the surface-integral method[15] in the case of homogeneous rough-surface scattering. In Fig. 2 we plot the DRC of one realization of a rough surface made of glass in the optical domain, with Gaussian statistics,[16] calculated with both methods. The rms height δ of the surface is $0.1\lambda_1$; the correlation length $a = \lambda_1$. The length along the x axis of the perturbed region is $L = 16\lambda_1$. Good agreement is obtained for both s and p polarizations.

We now turn to a completely different formalism based on a mixed representation of boundary-integral equations.

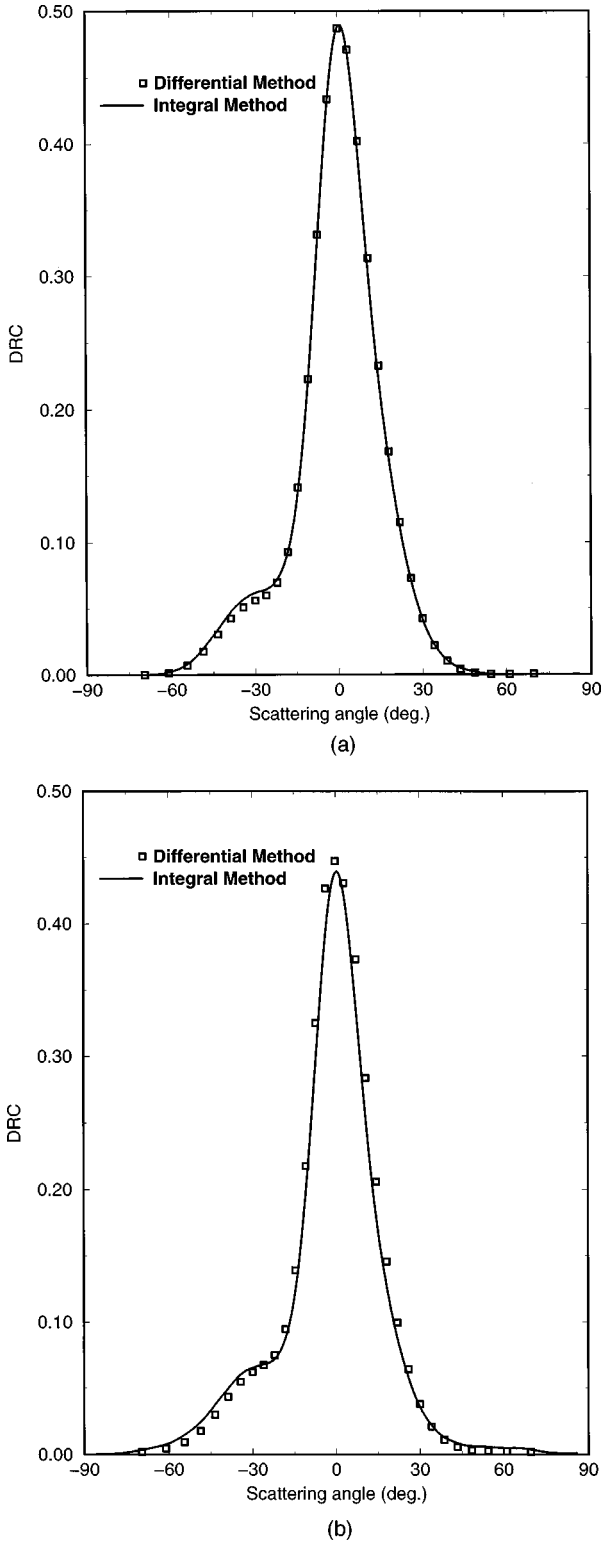

Fig. 2. DRC of a rough surface. $\delta = 0.1$, $a = 1$, $L = 16$, $\varepsilon_2 = 2.25$, $\lambda_1 = 1$. The waist of the incident beam is $w = 1$; normal incidence for (a) s polarization, (b) p polarization.

4. INTEGRAL METHOD

Surface integral methods were first developed to tackle scattering from homogeneous rough surfaces. Recently they were extended to more complicated geometries, such as a cylindrical object buried beneath a one-dimensional

rough surface.[12,17,18] This object may be either a bounded homogeneous scatterer or another rough interface separating two homogeneous media (Fig. 3). In this section we present an extension of the integral-boundary technique that is adapted to the case in which many small scatterers are present under a rough surface. The main advantage of the integral-boundary formalism as compared with the standard surface integral methods is that the former leads to a single-integral equation with single-scalar unknown, namely, a surface density along the boundaries. It is based on a single-layer representation

1. of the scattered field in the upper medium Ω_1, with density ϕ_1,

$$F(P) = F_{\text{inc}} + \int_{C_1} G_1(P, M')\phi_1(M')\mathrm{d}s', \quad \text{if } P \in \Omega_1, \tag{19}$$

where G_j denotes the free-space Green's function with wave number k_j, proportional to the Hankel function of zero order $G_j(P, M') = -\frac{i}{4} H_0^{(1)}(k_j PM')$ and F represents either the electric or the magnetic field, depending on whether the polarization is s or p, respectively;

2. of the total field in Ω_2, with density ϕ_2,

$$F(P) = \int_{C_2} G_2(P, M')\phi_2(M')\mathrm{d}s', \qquad \text{if } P \in \Omega_2. \tag{20}$$

Note that Eq. (19) is equivalent to Eq. (5a) when the Green's function is written in the Fourier space. Taking the limits when P tends to the boundary and taking into account the boundary conditions, we obtain the value of the field on the boundary and the limits of its normal derivative as a function of ϕ_1 and ϕ_2. Finally, applying the Green's theorem in Ω and taking the limit on the boundaries, we obtain

$$\frac{1}{2} F(M) = \int_{C_1 \cup C_2} \left[-G(M, M') \left(\frac{\mathrm{d}F}{\mathrm{d}n'} \right)_{\Omega} (M') + F(M') \frac{\mathrm{d}G}{\mathrm{d}n'} (M, M') \right] \mathrm{d}s', \quad M \in C_1 \cup C_2, \tag{21}$$

and can thus derive the integral equation with unknown ϕ_1 on C_1 and ϕ_2 on C_2. In Eq. (21) the normal is directed toward the exterior of Ω. The equation is transformed into a set of linear equations thanks to a boundary finite-element method. To ensure accuracy, the singular part of the kernels is extracted and analytically integrated. Also, to restrict the integration to a finite-domain interval with length L, the incident field has to vanish when x goes to infinity. With this goal we use incident Gaussian beams [Eq. (3)]. The method was tested against classical criteria, such as energy balance or reciprocity theorem, and compared with other methods.[12]

However, as a strong shortcoming, when the number of embedded scatterers is increased, both memory size and computation time increase rapidly. Therefore we have developed a new method that drastically reduces the number of unknowns, at least in the case of scatterers with dimensions smaller than the wavelength. Our method is based on the opportunity of describing the field that is scattered by a small object with a small number of terms in the Rayleigh expansion. As a counterpart, to remain rigorous, the method also requires knowledge of the scattering matrix of the object. Then including this object in any scattering problem introduces the significant Rayleigh coefficients as new unknowns. For instance, in the low-frequency range and s polarization, a cylindrical scatterer radiates an almost isotropic electric field, accurately described by a single complex number, thus leading to a single additional unknown. The same problem solved with a boundary finite-element method typically requires 10 to 20 unknowns, while the singularity of the kernels must be treated with care. Therefore a mixed representation of the scattered field is used: an integral representation for the contribution from the surface density lying on the rough interface and a Rayleigh expansion for the volume-scattering part.

Let us consider a set of scatterers $(\Omega_j)_{j>1}$ bounded by $(C_j)_{j>1}$, and an associated set of local systems of coordinates $O_j xz$, with the origin O_j located inside Ω_j. The local polar coordinates of a point P are given by $r_j = O_j P$ and $\theta_j = (O_j x, O_j P)$. Denoting by F_j^R the Rayleigh expansion of the field scattered by the jth rod in terms of outgoing Hankel functions, we get

$$F_j^R(P) = \sum_{n=-\infty}^{+\infty} b_n^{(j)} H_n^{(l)}(kr_j)\exp(\mathrm{i}n\theta_j), \tag{22}$$

where k represents the wave number in the surrounding medium. This expression is valid outside the smallest circle centered at O_j including Ω_j. If the Bessel functions are chosen as a basis for the description of the field F_j^{imp} impinging on the jth rod, we obtain

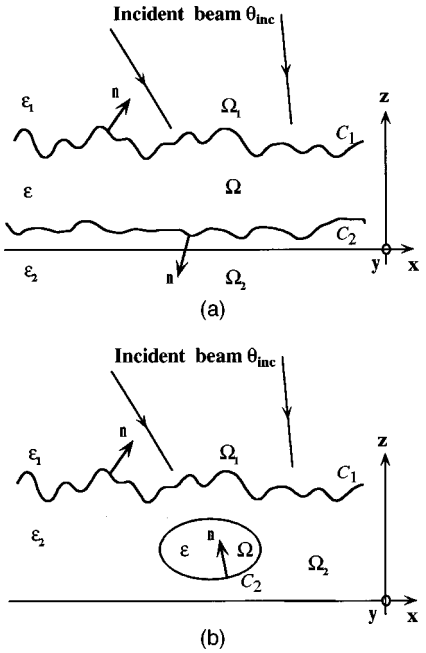

Fig. 3. Geometry of the problems: (a) stack of two rough interfaces, (b) buried cylindrical object under a rough surface. The structures considered are invariant along the y axis.

$$F_j^{\text{imp}}(r_j,\ \theta_j) = \sum_{n=-\infty}^{+\infty} a_n^{(j)} J_n(kr_j)\exp(\text{in}\theta_j), \qquad (23)$$

while the incident and scattered complex amplitudes, $a_n^{(j)}$ and $b_n^{(j)}$, respectively, are linked through the scattering matrix $\underline{\mathbf{S}}^{(j)}$.

Because we keep the same integral representation [Eq. (19)] for surface scattering, Eq. (21) becomes, when $M \in C_1$,

$$\frac{1}{2} F(M) = \int_{C_1} \left[-G(M, M') \left(\frac{\mathrm{d}F}{\mathrm{d}n'} \right)_{\Omega} (M') + F(M') \frac{\mathrm{d}G}{\mathrm{d}n'} (M, M') \right] \mathrm{d}s' + \sum_{j>1} F_j^R(M). \qquad (24)$$

This equation is rigorous, provided that one can plot disjointed circles centered at $(O_k)_{k>1}$ that include Ω_k and do not intersect C_1. It gives a first set of relationships between the surface density and the scattering amplitudes $b_n^{(j)}$, whose dimension is equal to the number of finite elements used to describe the surface profile. Note that in Eq. (24) there are more unknowns than equations. To complete the system, one writes additional equations that link the scattering amplitudes $b_n^{(j)}$ to the field impinging on the rods. With this aim, our first step consists in projecting this impinging field, namely, $F(P) - F_j^R(P)$ evaluated in the vicinity of O_j for the jth rod, onto the local basis of incident fields $J_n(kr_j)\exp(\text{in}\theta_j)$. This allows us to express the incident amplitudes as a function of the surface density and the $b_n^{(p)}$ $(p \neq j)$. In a second step we introduce the scattering matrix $\underline{\mathbf{S}}$ to link the incident amplitudes to the scattering ones. The resulting relationships, which couple the scattering amplitudes to the surface density, close the system. A matrix inversion is then used to evaluate both the surface density and the $b_n^{(p)}$.

To simplify the equations, let us assume that the jth scatterer is small and that the incident wave is s polarized. In such conditions $F_j^R(P)$ is well described by the central term ${b_0}^{(j)}$ of the expansion, and only knowledge of ${a_0}^{(j)}$ is needed. Because $J_0(kr_j)$ is the only Bessel function that does not vanish at O_j, ${a_0}^{(j)}$ is nothing but

$${a_0}^{(j)} = (F - F_j^R)(O_j). \qquad (25)$$

Therefore, provided the scattering matrix $\underline{\mathbf{S}}^{(j)}$ is known, we get a relationship coupling the surface density and the scattering amplitude ${b_0}^{(j)}$:

$${b_0}^{(j)} = {S_{00}}^{(j)} \int_{C_1} \left[-G(O_j, M') \left(\frac{\mathrm{d}F}{\mathrm{d}n'} \right)_{\Omega} (M') + F(M') \frac{\mathrm{d}G}{\mathrm{d}n'} (O_j, M') \right] \mathrm{d}s' + {S_{00}}^{(j)} \sum_{p \neq j} {F_p}^R(O_j). \qquad (26)$$

When j is varied, the number of equations given by Eq. (26) is equal to the number of unknown scattering amplitudes. Consequently, Eqs. (24) and (26) lead to a linear set with the same number of equations and unknowns. The derivation of the scattering amplitude in the upper medium, expressed as a function of the surface density ϕ_1, remains unchanged:

$$f_1(\alpha) = \frac{-i}{4\pi\gamma_1(\alpha)} \int \phi_1(\alpha)\exp[-i\alpha x' - i\gamma_1(\alpha)z']\mathrm{d}s'. \qquad (27)$$

The validity of this approach is tested by comparison of the DRC of a rod placed below a flat surface with the results given by the boundary-integral method [see Fig. (4)]. The circular rod with a diameter of $\lambda_1/20$ and a relative permittivity of $\varepsilon = 5$ is centered at $\lambda_1/20$ below a flat in-

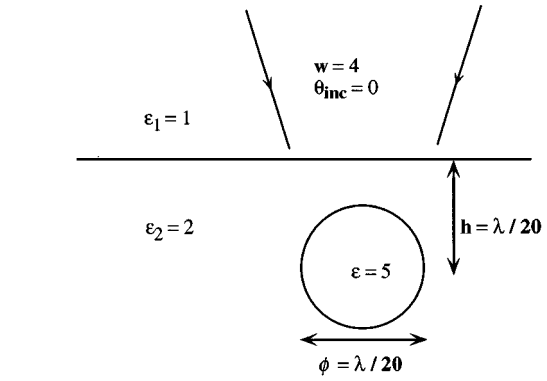

(a)

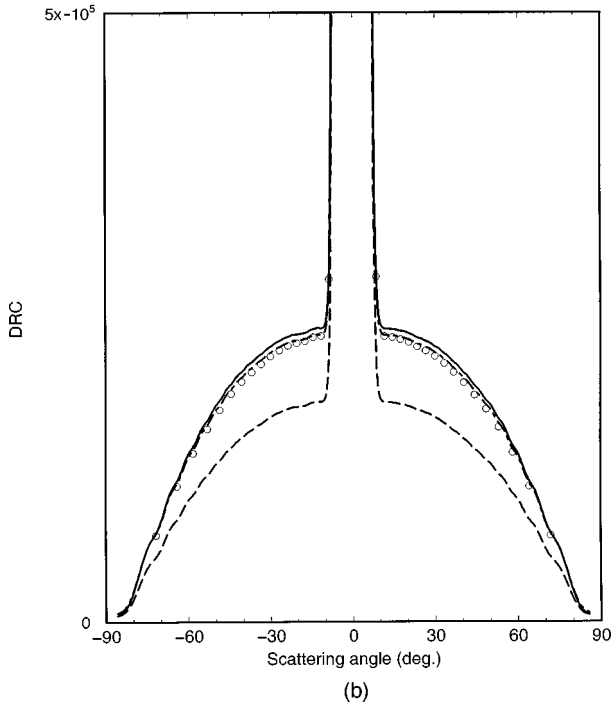

(b)

Fig. 4. (a) Buried object (cylinder) under a flat surface. (b) Comparison between a boundary finite-element description and the mixed representation. Dashed curve, 5 elements are used to describe the rod; dotted–dashed curve, 15 elements are used to describe the rod. Solid curve, 50 elements are used to describe the rod (convergence reached); dotted curve, mixed representation with one term in the Rayleigh expansion.

terface separating vacuum (up) from a semi-infinite medium with a permittivity of $\varepsilon_2 = 2$. The incident field is described by an s-polarized Gaussian beam with normal incidence and a waist of $w = 4$. Note that one gets the same accuracy (2%) with one scattering amplitude (i.e., one term in the Rayleigh expansion) as with 15 boundary elements. This permits one to solve scattering problems with a great number of small scatterers with low computational cost.

5. NUMERICAL RESULTS

To check the validity of the methods described in Sections 3 and 4 and to point out their wide range of application, we have studied the scattering from different kinds of structures and drawn comparisons. In all the calculations presented in this section the wavelength of the incident light is $\lambda_1 = 1$. The upper medium is air with $\varepsilon_1 = 1$.

We have computed the DRC of a structure composed of a buried object under a rough surface in a deterministic case (Fig. 5). This calculation corresponds to a remote sensing experiment. One can see in Fig. 6 the angular pattern of the scattered light obtained with both methods. A good agreement is found between the two results.

We have also studied the scattering from a structure composed of 87 scatterers, whose diameter is equal to $\lambda_1/20$, buried in a homogeneous medium under a rough surface (Fig. 7). The computations were made for two different values of the permittivity ε_s of the scatterers. For $\varepsilon_s = 3.15$ the parameters of the considered geometry are similar to those of the snow at 17 GHz described in Ref. 19. One can see that, as expected, when the value of ε_s is increased, the scattering becomes stronger [see Fig. 7(b)]. Figure 7 shows that once again a good agreement is found between the two methods. In light of the results of Figs. 2, 6, and 7, it seems clear that these methods permit one to handle both surface and volume scattering.

We now focus on the differential method whose versatility and ease of implementation are worth emphasizing. We have calculated the scattering from a snow layer (see Fig. 8) as described in Ref. 19. The scattering problem involves many small scatterers (cylinders in a structure invariant along the y axis) and two uncorrelated rough interfaces. In this stochastic case the mean DRC was calculated by averaging over 50 realizations. The results of Fig. 9 show that the amount of scattered light depends on the density of scatterers. We have also studied another model for the snow layer (Fig. 10) corresponding to that given in Refs. 20–22. In this model the snowcover is described by an inhomogeneous layer sandwiched between two identical rough surfaces. The permittivity of the layer satisfies the equation $\varepsilon(x, z) = 1.57 + 10^{-1}d$, where $d(x, z)$ is the distance of the point (x, z) to the up-

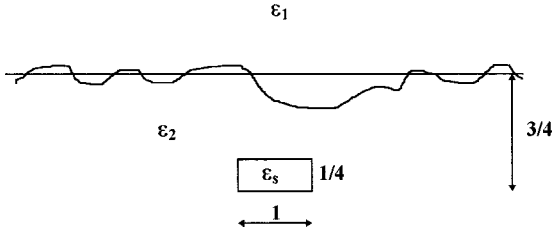

Fig. 5. Buried object (cylinder) under a rough surface. The structures considered are invariant along the y axis.

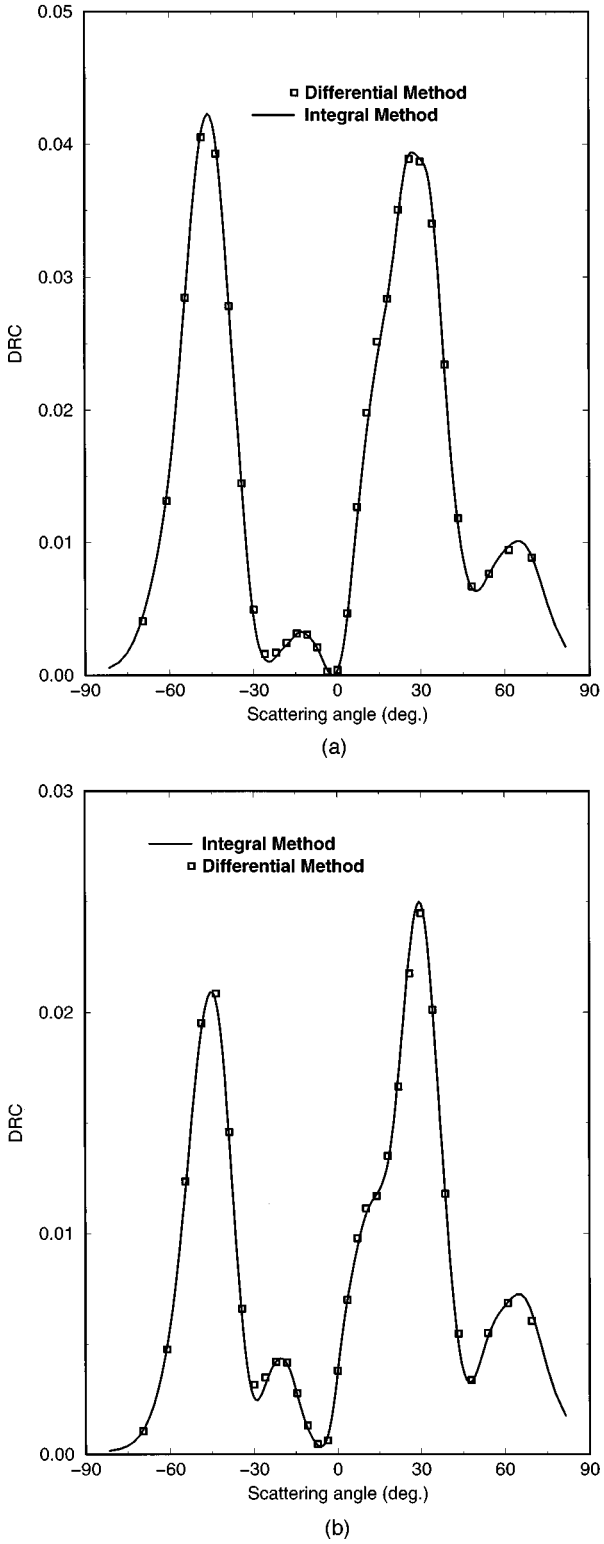

Fig. 6. DRC of the structure shown in Fig. 5: $\delta = 0.1$, $a = 1$, $L = 16$, $\varepsilon_2 = 2.25 + 10^{-2}i$, $\varepsilon_3 = 9$. ε is ε_2 in the bulk and ε_s in the scatterer. The waist of incident beam is $w = 1$. Normal incidence for (a) s polarization, (b) p polarization.

per interface. Figure 11 shows the angular pattern of the scattered light for two different thicknesses H of the snow layer. The total amount of scattered light depends on H. We can use this property to determine the thickness of the snow layer by comparing experimental data given by a remote sensing technique with the numerical

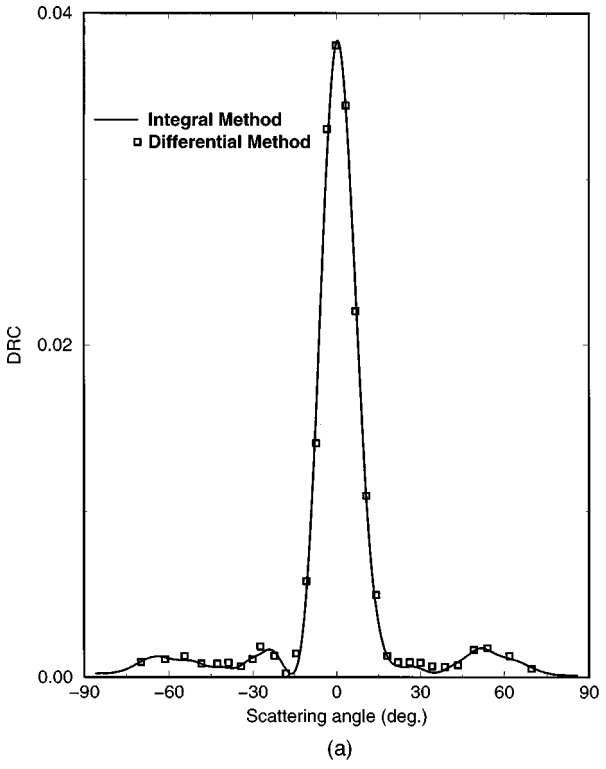

Fig. 7. DRC of a rough inhomogeneous medium with 87 cylindrical scatterers randomly distributed. $\delta = 0.1$, $a = 1$, $L = 16$, $\varepsilon_2 = 1.482$. Thickness of the nonhomogeneous region, $D = 0.6$; diameter of the scatterers. $\phi = \lambda_1/20$; waist of the incident beam: $w = 1$. Normal incidence and S polarization for (a) $\varepsilon_s = 3.15$, (b) $\varepsilon_s = 9$.

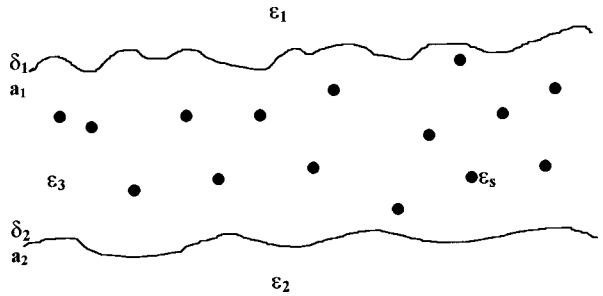

Fig. 8. Model of the snow layer. Structures considered are invariant along the y axis. Diameter of the scatterers is $\phi = \lambda_1/30$. $\delta_1 = 8.10^{-2}$, $a_1 = 4.10^{-1}$, $\delta_2 = 3.10^{-2}$, $a_2 = 1.6.10^{-1}$, $\varepsilon_2 = 5$, $\varepsilon_3 = 1.482$, $\varepsilon_s = 3.15$; ε is ε_3 in the bulk and ε_s in the scatterer.

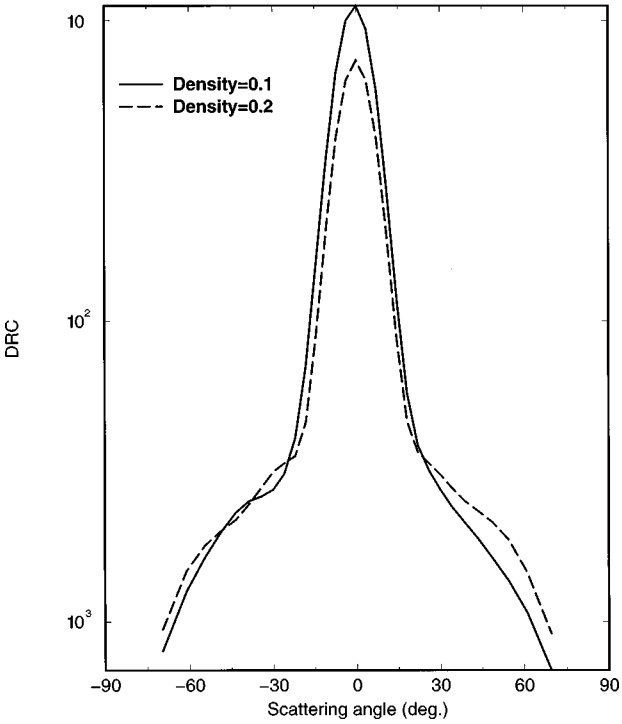

Fig. 9. DRC of the structure described in Fig. 8 for two densities (in volume) of the scatterers. Scatterers are randomly distributed. Average of 50 realizations. The waist of the incident beam is $w = 1$. Normal incidence for s polarization.

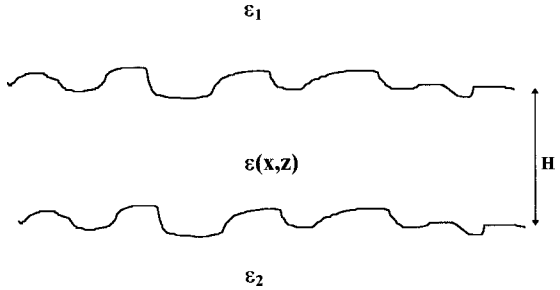

Fig. 10. Model of the snow layer as a graded index medium. The upper surface and the lower surface are identical. $\delta = 0.1, a = 1, L = 25$; $\varepsilon_2 = 5$; $\varepsilon(x, z) = 1.57 + 10^{-1}d$, where d is the distance of the point (x, z) from the surface.

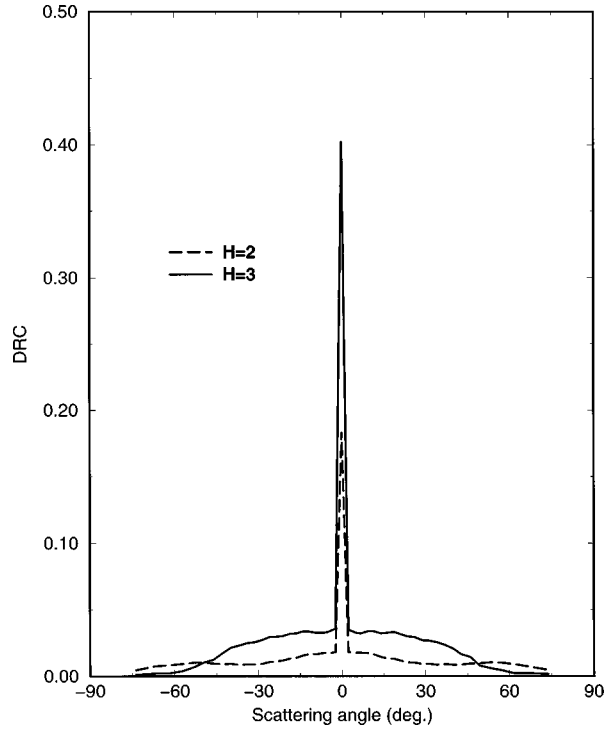

Fig. 11. DRC of the structure described in Fig. 10. Average of 200 realizations, plane incident wave. Normal incidence for *s* polarization.

results obtained with the differential method. Some approximate models have been proposed to calculate scattering from this kind of structure,[23] but, to our knowledge, no methods based on a rigorous formulation of Maxwell's equations have been proposed to solve this problem. Although examples are given here in the radio-frequency domain, the methods described in Sections 3 and 4 can also be used to compute scattering from paints (which can be considered rough inhomogeneous media) in an optical domain.[2,24]

6. CONCLUSION

Two methods capable of calculating the scattering from rough one-dimensional inhomogeneous films have been presented and compared. We have shown that, thanks to a mixed representation in the coordinate and spectral domains, both surface and volume scattering can be handled with a boundary-integral method. We have also extended the fields of application of the differential methods to the problem of scattering from rough inhomogeneous films. These methods have been applied to the study of scattering from snowcovers or objects buried under a rough surface illuminated by a Gaussian beam. Note that when the incident beam is large, the beam simulation method[25] can be implemented in both cases.

The derivation of the propagation equation in the Fourier space (differential method) permits one to study the scattering from a wide range of structures, such as stacks of rough inhomogeneous films with interpenetrating layers, overhanged rough surfaces, graded index media, etc., that are difficult to treat with an integral method. Moreover, if we assume that the computer memory size is sufficient, the extension of the differential method to the three-dimensional problem is immediate,[26] as no singularities of the functions used in the set of coupled differential equations have to be handled during integration. The price to pay for these potentialities is the time of computation, which is nearly ten times longer than that of the integral method described in this paper.

Consequently, the two methods presented in this paper appear to be complementary, and, in addition to the applications shown in this paper, they can be used to study near-field and enhanced backscattering from rough inhomogeneous structures.

REFERENCES

1. H. Kaplan, "Black coatings are critical in optical design," Phot. Spec. **31**, 48–50 (1997).
2. H. Giovannini and C. Amra, "Scattering-reduction effect with overcoated rough surfaces: theory and experiment," Appl. Opt. **36**, 5574–5579 (1997).
3. J. M. Elson, "Theory of light scattering from a rough surface with an inhomogeneous dielectric permittivity," Phys. Rev. B **30**, 5460–5480 (1984).
4. A. Fung, "First-order radiative transfer solution—active sensing," in *Microwave Scattering and Emission Models and Their Applications*, F. T. Ulaby, ed. (Artech House, Boston, 1994), Chap. 2, pp. 49–122.
5. C. Amra, "First-order vector theory of bulk scattering in optical multilayers," J. Opt. Soc. Am. A **10**, 365–374 (1993).
6. S. Dietrich and A. Haase, "Scattering of x-rays and neutrons at interfaces," Phys. Rep. **260**, 1–138 (1995).
7. K. Sarabandi, Y. Oh, and F. T. Ulaby, "A numerical simulation of scattering from one-dimensional inhomogeneous dielectric random surfaces," IEEE Trans. Geosci. Remote Sens. **34**, 425–432 (1996).
8. L. Rakotoarivony, O. Taconet, D. Vidal-Madjar, P. Bellemain, and M. Benallegne, "Radar backscattering over agricultural bare soils," J. Electron. Waves Appl. **10**, 187–210 (1996).
9. P. Vincent, "Differential methods," in *Progress in Optics XXII*, E. Wolf, ed. (Springer-Verlag, Berlin, 1980), pp. 101–121.
10. L. Li, "Formulation and comparison of two recursive matrix algorithms for modeling layered diffraction gratings," J. Opt. Soc. Am. A **13**, 1024–1035 (1996).
11. F. Montiel and M. Nevière, "Differential theory of gratings: extension to deep gratings of arbitrary profile and permittivity through the *R*-matrix algorithm," J. Opt. Soc. Am. A **11**, 3241–3250 (1994).
12. M. Saillard and G. Toso, "Electromagnetic scattering from bounded of infinite subsurface bodies," Radio Sci. **32**, 1347–1359 (1997).
13. K. Pak, L. Tsang, L. Li, and C. H. Chan, "Combined random rough surface and volume scattering based on Monte Carlo simulations of solutions of Maxwell's equations," Radio Sci. **28**, 331–338 (1993).
14. J. P. Hugonin and R. Petit, "A numerical study of the problem of diffraction at a non-periodic obstacle," Opt. Commun. **20**, 360–363 (1977).
15. M. Saillard and D. Maystre, "Scattering from metallic and dielectric rough surfaces," J. Opt. Soc. Am. A **7**, 982–990 (1990).
16. A. A. Maradudin, T. Michel, A. R. Mc Gurn, and E. R. Méndez, "Enhanced backscattering of light from a random grating," Ann. Phys. (New York) **203**, 255–276 (1990).
17. A. Madrazo and M. Nieto-Vesperinas, "Scattering of light and other electromagnetic waves from a body buried beneath a highly rough random surface," J. Opt. Soc. Am. A **14**, 1–8 (1997).

18. K. O'Neill, R. F. Lussky, Jr., and K. D. Paulsen, "Scattering from a metallic object embedded near the randomly rough surface of a lossy dielectric," IEEE Trans. Geosci. Remote Sens. **34**, 367–376 (1996).
19. A. Fung, "Scattering and emission models for snow and sea ice," in *Microwave Scattering and Emission Models and Their Applications*, F. T. Ulaby, ed. (Artech House, Boston, 1994), Chap. 9, p. 382.
20. C. Mätzler, "Applications of the interaction of microwaves with the natural snowcover," Remote Sens. Rev. **2**, 259–392 (1987).
21. M. E. Tiuri, A. H. Sihvola, E. G. Nyfors, and M. T. Hallikainen, "The complex dielectric constant of snow at microwave frequencies," IEEE J. Oceanic Eng. **OE-9**, 377–382 (1994).
22. S. Surdyk and M. Fily, "Results of a stratified snow emissivity model based on the wave approach: application to the Antarctic sheet," J. Geophys. Res. **100**, 8837–8848 (1995).
23. K. Sarabandi and T. Chiu, "Electromagnetic scattering from slightly rough surfaces with inhomogeneous dielectric profiles," IEEE Trans. Antennas Propag. **45**, 1419–1430 (1997).
24. H. Giovannini and C. Amra, "Enhanced absorption in very rough overcoated black surfaces," *International Symposium on Optical Science, Engineering, and Instrumentation, San Diego*, Proc. SPIE **3133**, (1997), pp. 110–114.
25. M. Saillard and D. Maystre, "Scattering from random rough surfaces: a beam simulation method," J. Opt. (Paris) **19**, 173–176 (1988).
26. P. Vincent, "A finite-difference method for dielectric and conducting crossed gratings," Opt. Commun. **26**, 293–295 (1978).